

STRESS ANALYSIS MODELS OF HUMAN LONG BONES - ANALYTIC AND FINITE ELEMENT APPROACHES

Paulo Pedro Kenedi, pkenedi@cefet-rj.br

Ivan Ivanovitsch Thesi Riagusoff, ivanthesi@yahoo.com.br

CEFET/RJ – Department of Mechanical Engineering – Av. Maracanã, 229 – Maracanã – CEP 20271-110 – Rio de Janeiro - Brasil

***Abstract.** Many works have been published applying finite element method to estimate stresses generated by the application of various types of loading at long bones. Although this approach has many advantages, the relationship between the main variables are not shown. Analytic models does establish an explicit relationship between loads and stresses, which is intrinsically advantageous as relates causes and effects. These analytic models are built in a increase level of complexity, in fuction of cross section improvements, to come close to a real cross section of a long bone. A comparative study between these analytic models are implemented to analyze the effect of increse of model complexity on its performance, using as reference a finite element model.*

***Keywords:** long bones, stress analysis, analytic model*

1. INTRODUCTION

Two analytic models of stress analysis of long bones, like a femur, shown in this work represent the conclusion of a research initiated by the authors at former works (Kenedi, 2009), (Kenedi, 2008), (Kenedi, 2007a) and (Kenedi, 2007b). In this work many expressions were recast in sake of simplicity and compact presentation. Two models of cross sections were utilized: a hollow circle and a hollow ellipse, both with constant thickness. The hollow circle model is easier to apply but describes roughly a real long bone cross section whereas the hollow ellipse model is more complex and laborious to apply but represent better a real long bone cross section. The mathematical manipulations are kept at an introductory level as well as the application of the theory of mechanics of solids.

As done at former works, several limiting hypotheses have to be made in order to assure the viability of these models. For instance, only cortical bone is utilized (the trabecular tissue is not included). Loading conditions are static. Restraints are positioned only at extremities of long bones, no side ligaments or muscles are recognized. The analysis is made at medial cross section, therefore far from long bone ends.

A well establish commercial Element Finite software was used to generate reference results to compare with the analytic models results.

2. ANALYTIC MODELS

Two analytic models of stress analysis of cross section at medial long bone, are developed, one with hollow circle and other with hollow ellipse cross sections, both with constant thickness. The first takes advantage of evident symmetry, which simplifies the model expressions. The second maintain only two symmetries, which turn the model rather complex, but closer to a real long bone cross section. Although the models expressions have straightforward application, its calculations are rather tedious, requiring the utilization of mathematical software, like MathCad.

The description of the two models are done in the following sequence: first is shown the equivalent loading at a medial cross section of, for example, a femur's head loading, secondly the expressions that relates loads and stresses are cast, and finally these stresses are rewritten in function of principal and maximum shear stresses by the utilization of Mohr Circle approach. The first step is pretty much the same for the two models, the second step is fully developed for each model and the last step are common for the two analytic models.

Although mechanics of solids was used only at an introductory level, the cross section geometry, especially for the hollow ellipse model, generates a relatively complex set of expressions. Also, the hollow ellipse model uses two axis systems, a local that accompanies the long axis of the cross section and a global one that always maintains its initial configuration.

The separate estimation of axial, bending, transverse shear and torsional stresses is one goal of the utilization of analytic models, as is possible to estimate the most significant stress at a given point of external surface of a long bone cross section submitted to a given loading condition. This gain importance because enables attempts to relate loading to types of failure thought the estimation which stresses are important. Another goal of application of these analytic models is the generation of principal stresses and maximum shear stresses, which are key variables to failure criteria, even though until nowadays the research to establish a criterion of failure for long bones is still in course.

2.1 – Loading at cross section

Figure 1 shows an example of human femur hypothetical cut at a generic medial section. At a distance d away from the centre of the generic medial cross section a static force \mathbf{P} , represented by its components, loads femur's head.

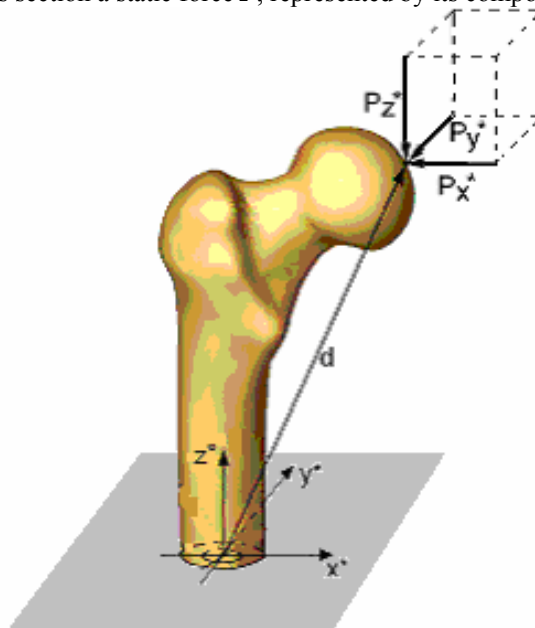


Figure 1. An example of a static load of a human femur's head.

The static force \mathbf{P} is represented by its components in global coordinates system:

$$\mathbf{P} = P_x^* \vec{i} + P_y^* \vec{j} + P_z^* \vec{k} \quad (1)$$

At the chosen cross section, the components of force are:

$$\begin{aligned} V_x &= P_x^* \\ V_y &= P_y^* \\ V_z &= P_z^* = N \end{aligned} \quad (2)$$

The components of moments are:

$$\begin{aligned} M_x^* &= d_y P_z^* - d_z P_y^* \\ M_y^* &= d_z P_x^* - d_x P_z^* \\ M_z^* &= d_x P_y^* - d_y P_x^* = T \end{aligned} \quad (3)$$

where,

$$\mathbf{d} = d_x \vec{i} + d_y \vec{j} + d_z \vec{k} \quad (4)$$

The variables presented in bold are vectors, the components of vectors that have an asterisk are referenced to global system of coordinates. N is the axial force, V is the shear force, M is the bending moment and T is the torsional moment. \vec{i} , \vec{j} and \vec{k} are unit vectors.

2.2 – Hollow circle model

The first analytic model estimate the distribution of stresses at external surface of a medial hollow circle cross section of a long bone (Kenedi, 2007a) and (Kenedi, 2007b). Figure 2 shows the geometry and the main variables of this model.

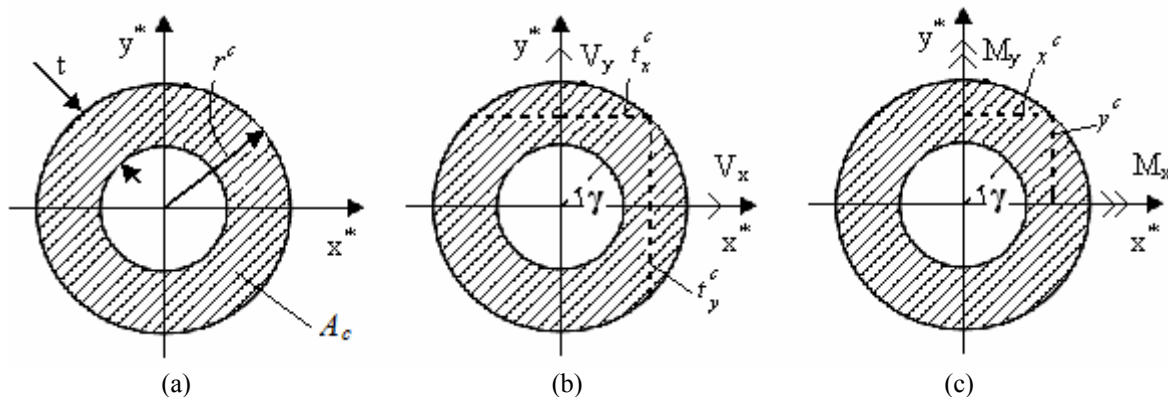


Figure 2. (a) Geometric variables, (b) transverse shear variables and (c) bending variables of a hollow circle cross section of a long bone.

Figure 2.a shows the cross sectional area A_c , the external radius r^c and thickness t , fig.2.b shows the angle γ that defines the point of interest at external surface of a given cross section (where $\gamma = 0^\circ$ at positive x^* axis), t_y^c and t_x^c are respectively the width of bone, at point of interest, perpendicular, respectively, to x^* and y^* axis. At fig. 2.c y^c and x^c are respectively, the perpendicular distances from axis x^* and y^* to external bone surface.

The axial stress σ_N is (Crandall, 1978):

$$\sigma_N = \frac{N}{A_c} \quad (5)$$

where, $A_c = \frac{\pi t}{4}(2r^c - t)$ (6)

The bending stresses components, σ_{F_x} and σ_{F_y} are (Crandall, 1978):

$$\sigma_{F_x} = \frac{M_x^* y^c}{I_x^c} \quad \text{and} \quad \sigma_{F_y} = \frac{M_y^* (-x^c)}{I_y^c} \quad (7)$$

$$x^c = r^c \cos(\gamma) \quad \text{and} \quad y^c = r^c \sin(\gamma) \quad (8)$$

$$I_x^c = I_y^c = \frac{\pi}{4} \left((r^c)^4 - (r^c - t)^4 \right) \quad (9)$$

where, M_x^* and M_y^* are bending moments components and I_x^c and I_y^c are, respectively, the second moment of area about x^* and y^* axis.

The torsional stress τ_T is (Crandall, 1978):

$$\tau_T = \frac{Tr^c}{J_c} \quad (10)$$

$$J_c = \frac{\pi}{2} \left((r^c)^4 - (r^c - t)^4 \right) \quad (11)$$

where, J_c is the polar second moment of area.

The transverse shear stress components τ_{v_x} and τ_{v_y} are (Crandall, 1978):

$$\tau_{v_x} = \frac{V_x Q_y^c}{I_y^c t_y^c} \text{ and } \tau_{v_y} = \frac{V_y Q_x^c}{I_x^c t_x^c} \quad (12)$$

where,

$$t_x^c = 2r^c \sqrt{1 - \left(\frac{y^c}{r^c}\right)^2} - \left[2(r^c - t) \sqrt{1 - \left(\frac{y^c}{r^c - t}\right)^2} \right] k_x \quad \text{and} \quad t_y^c = 2r^c \sqrt{1 - \left(\frac{x^c}{r^c}\right)^2} - \left[2(r^c - t) \sqrt{1 - \left(\frac{x^c}{r^c - t}\right)^2} \right] k_y \quad (13)$$

$$Q_x^c = \int_{y^c}^{r^c} 2r^c y \sqrt{1 - \left(\frac{y^c}{r^c}\right)^2} dy - \left[\int_{(r^c - t) \sin(\gamma)}^{r^c - t} 2(r^c - t) y \sqrt{1 - \left(\frac{y^c}{r^c - t}\right)^2} dy \right] k_x \quad (14)$$

$$Q_y^c = \int_{x^c}^{r^c} 2r^c x \sqrt{1 - \left(\frac{x^c}{r^c}\right)^2} dx - \left[\int_{(r^c - t) \cos(\gamma)}^{r^c - t} 2(r^c - t) x \sqrt{1 - \left(\frac{x^c}{r^c - t}\right)^2} dx \right] k_y$$

where, V_x and V_y are shear force components, Q_x and Q_y are, respectively, the first moment of area about x^* and y^* axis.

t_x^c and t_y^c are respectively the width of bone, at point of interest, perpendicular, respectively, to x^* and y^* axis. Note that $k_x = 0$ for $|y^c| \geq (r^c - t)$, $k_x = 1$ otherwise, and $k_y = 0$ for $|x^c| \geq (r^c - t)$, $k_y = 1$ otherwise.

2.3 – Hollow ellipse model

The second analytic model estimates the distribution of stresses at external surface of a medial hollow ellipse cross section of a long bone (Kenedi, 2009) and (Kenedi, 2008). Figure 3 shows the geometry and the coordinate systems of this model.

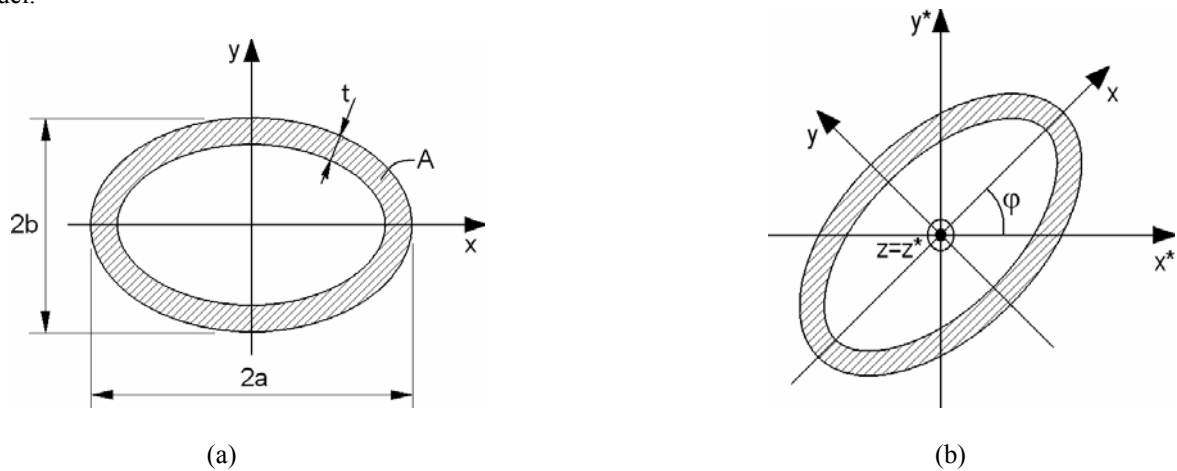


Figure 3. (a) Idealized hollow ellipse cross section of a long bone and (b) local and global coordinate systems.

Figure 3.a shows a hollow ellipse cross section, with constant thickness t , with long axis $2a$ and short axis $2b$, and cross sectional area A . Fig. 3.b shows two coordinates systems: local and global. The local coordinates (x, y, z) are attached to cross section, where x and y axis are respectively, coincident with $2a$ and $2b$ axis. The z axis is obtained by the application of the *right-hand rule*. Each cross section has its own local axis configuration, always maintaining x axis coincident with $2a$. Global coordinates (x^*, y^*, z^*) has always the same orientation in space, where $x^* y^*$ is a horizontal plane, $x^* z^*$ and $y^* z^*$ are vertical planes. φ is the angle between coordinate systems.

The force components, written in local coordinates, are:

$$\begin{aligned} V_x &= P_x^* \cos(\varphi) + P_y^* \sin(\varphi) \\ V_y &= -P_x^* \sin(\varphi) + P_y^* \cos(\varphi) \\ V_z &= N = P_z^* \end{aligned} \quad (15)$$

Moments components, written in local coordinates, are:

$$\begin{aligned} M_x &= M_x^* \cos(\varphi) + M_y^* \sin(\varphi) \\ M_y &= -M_x^* \sin(\varphi) + M_y^* \cos(\varphi) \\ M_z &= M_z^* = T \end{aligned} \quad (16)$$

Note that (2) and (3) expressions are a particular case of (15) and (16) expressions when $\varphi = 0^\circ$.

The axial stress σ_N is (Crandall, 1978):

$$\sigma_N = \frac{N}{A} \quad (17)$$

$$\text{where, } A = \pi t(a + b - t) \quad (18)$$

Figure 4 shows the bending, torsional and transverse shear variables of a hollow ellipse cross section of a long bone.

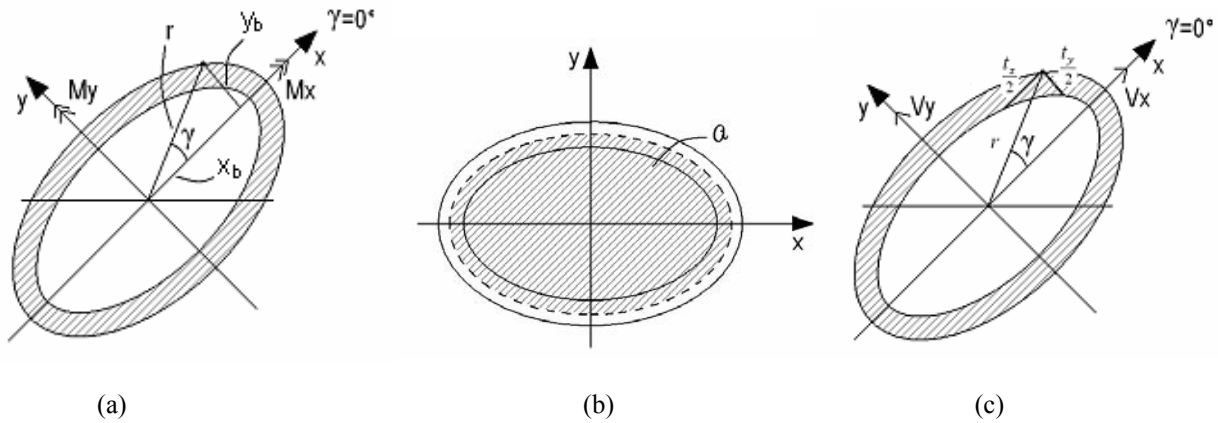


Figure 4. (a) Bending variables of a hollow ellipse cross section of a long bone, (b) torsional variables and (c) transverse shear variables of a hollow ellipse cross section of a long bone.

The bending stresses components, σ_{F_x} and σ_{F_y} , are (Crandall, 1978):

$$\sigma_{F_x} = \frac{M_x y_b}{I_x} \quad \text{and} \quad \sigma_{F_y} = \frac{M_y (-x_b)}{I_y} \quad (19)$$

$$x_b = r \cos(\gamma) \quad \text{and} \quad y_b = r \sin(\gamma) \quad (20)$$

$$I_x = \frac{\pi}{4} (ab^3 - (a-t)(b-t)^3) \quad \text{and} \quad I_y = \frac{\pi}{4} (a^3 b - (a-t)^3 (b-t)) \quad (21)$$

$$r_i(\gamma) = \sqrt{(a-t)^2 \cos^2(\gamma) + (b-t)^2 \sin^2(\gamma)} \quad \text{and} \quad r_o(\gamma) = \sqrt{a^2 \cos^2(\gamma) + b^2 \sin^2(\gamma)} \quad (22)$$

where, x_b and y_b are respectively, the perpendicular distances from axis y and x to external bone surface. M_x and M_y are bending moments components. I_x and I_y are second moment of area. r_o is the external radius, the distance from the centre of cross section to the point of interest at external surface of bone, and r_i is the internal radius.

The torsional stress τ_t is (Crandall, 1978):

$$\tau_t = \frac{T}{2t\Omega} \quad (23)$$

$$\Omega = \pi \left(a - \frac{t}{2} \right) \left(b - \frac{t}{2} \right) \quad (24)$$

where, T is the torsional moment and Ω is the area inside a line which passes in middle thickness of bone cross section.

The transverse shear stress components, τ_{v_x} and τ_{v_y} , are (Crandall, 1978):

$$\tau_{v_x} = \frac{V_x Q_y}{I_y t_y} \text{ and } \tau_{v_y} = \frac{V_y Q_x}{I_x t_x} \quad (25)$$

where,

$$t_x = 2a\sqrt{1-\left(\frac{y_b}{b}\right)^2} - \left[2(a-t)\sqrt{1-\left(\frac{y_b}{b-t}\right)^2}\right] k_x \text{ and } t_y = 2b\sqrt{1-\left(\frac{x_b}{a}\right)^2} - \left[2(b-t)\sqrt{1-\left(\frac{x_b}{a-t}\right)^2}\right] k_y \quad (26)$$

$$Q_x = \int_{y_b}^b 2ay\sqrt{1-\left(\frac{y_b}{b}\right)^2} dy - \left[\int_{\eta(\gamma)\sin(\gamma)}^{b-t} 2(a-t)y\sqrt{1-\left(\frac{y_b}{b-t}\right)^2} dy \right] k_x \quad (27)$$

$$Q_y = \int_{x_b}^a 2bx\sqrt{1-\left(\frac{x_b}{a}\right)^2} dx - \left[\int_{\eta(\gamma)\cos(\gamma)}^{a-t} 2(b-t)x\sqrt{1-\left(\frac{x_b}{a-t}\right)^2} dx \right] k_y$$

Note that $k_x = 0$ for $|y_b| \geq (b-t)$, $k_x = 1$ otherwise, and $k_y = 0$ for $|x_b| \geq (a-t)$, $k_y = 1$ otherwise.

2.4 – Mohr Circle

This subsection is common for the two analytic models and shows how transform the axial, bending, transverse shear and torsional stresses in principal and maximum shear stresses. The resultant normal stress and the resultant shear stress can be estimated as shown at (28) and (29) expressions:

$$\sigma_y = \sigma_N + \sigma_F \text{ and } \tau_{xy} = \tau_T + \tau_v \quad (28)$$

$$\text{where, } \sigma_F = \sigma_{F_x} + \sigma_{F_y} \text{ and } \tau_v = \tau_{v_x} + \tau_{v_y}. \quad (29)$$

To transform normal and shear stresses (non principal stresses) in principal stresses, and also to estimate the maximum shear stress, the Mohr circle is utilized.

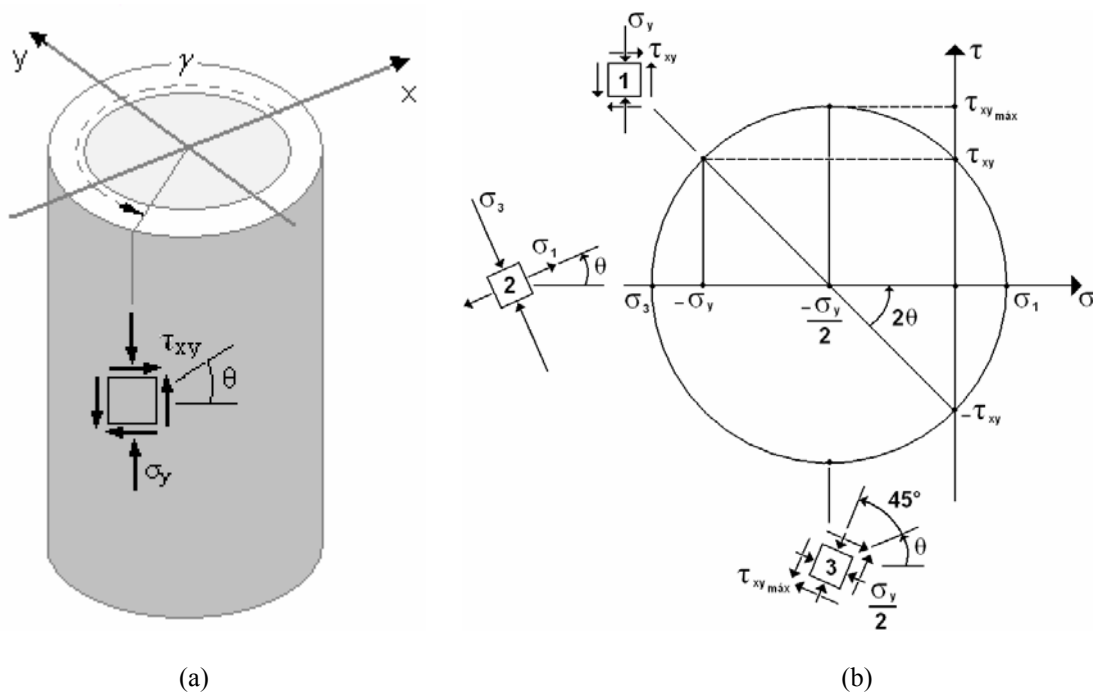


Figure 5. (a) Stresses at a point of external surface of a long bone and (b) Mohr circle.

The angle θ represents the orientation of the element of area (at figure $\theta = 0^\circ$). At fig. 5.b a Mohr circle is represented for three conditions numbered from 1 to 3, at same external surface point: The first one correspond to the actual situation shown at fig.5.a.

The second condition turns θ at external surface of long bone from its initial position (2θ at Mohr circle) to reach the angle of principal stresses. The third position, add 45° to second position (add 90° at Mohr circle) to reach the angle of maximum shear stresses. Note that at Mohr circle the angle θ is doubled (Crandall, 1978).

The principal stresses and angles at surface of a long bone are:

$$\sigma_1, \sigma_3 = \frac{\sigma_y}{2} \pm \sqrt{\left(\frac{\sigma_y}{2}\right)^2 + \tau_{xy}^2}, \theta = \frac{1}{2} \arctan\left(\left|\frac{2\tau_{xy}}{\sigma_y}\right|\right) \quad (30)$$

The maximum shear stress and angles at surface of a long bone are:

$$\tau_{\max} = \sqrt{\left(\frac{\sigma_y}{2}\right)^2 + \tau_{xy}^2}, \theta' = \theta + 45^\circ \text{ or } \theta' = \theta + 135^\circ \quad (31)$$

3. FINITE ELEMENT MODEL

A finite element model was implemented, with the utilization of a well known commercial FEM package. The results of application of this model were used as reference to compare the performance of analytic models. The geometry was imported into ANSYS Design Modeler from a Parasolid file format. Figure 6.a shows a representation of the geometry of finite element model with global coordinates, fig 6.b shows the loading condition, 6.c shows the chosen cross section and 6.d shows mechanical properties of cortical human femur bone (Rapoff, 2007).

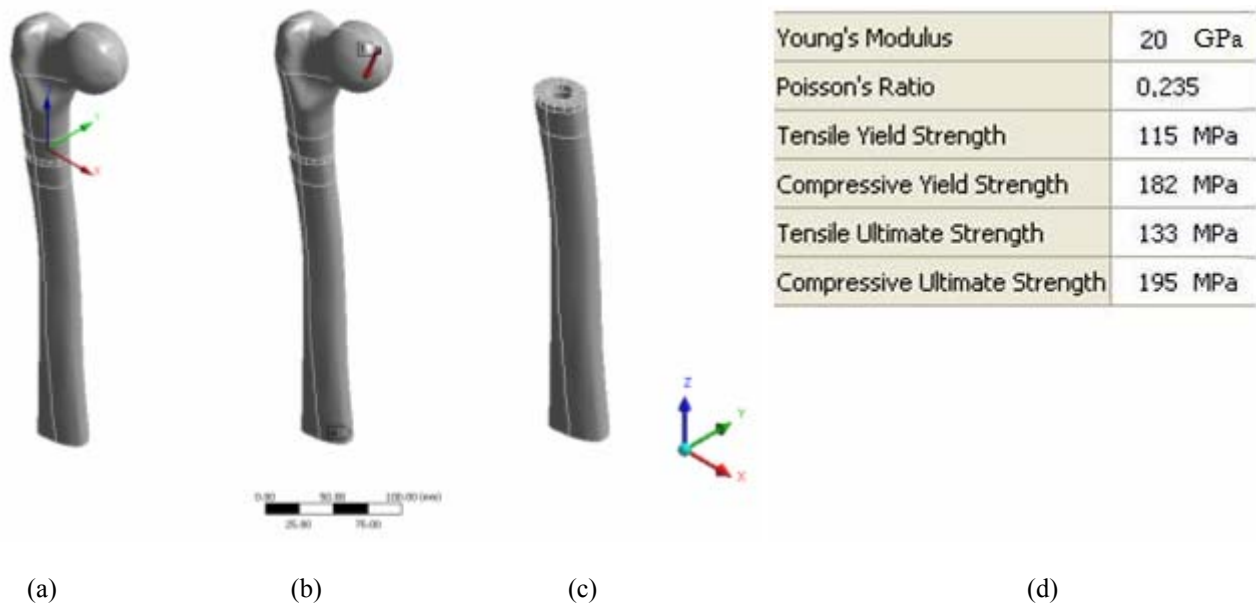


Figure 6. F.E. human femur model: (a) geometric model with global coordinates, (b) concentrated static loading at femur's head (red arrow), (c) view of the chosen cross section and (d) mechanical properties of a human femur.

The F.E. model of a human femur is linear and elastic, with little displacements and rotations. The geometry is quite complex, but could be imported from a real scanned human femur geometry.

Figure 7.a shows the mesh of geometric model and fig.7.b shows the refinement of mesh at the region of interest. It was used 30742 Nodes and 13295 Elements.

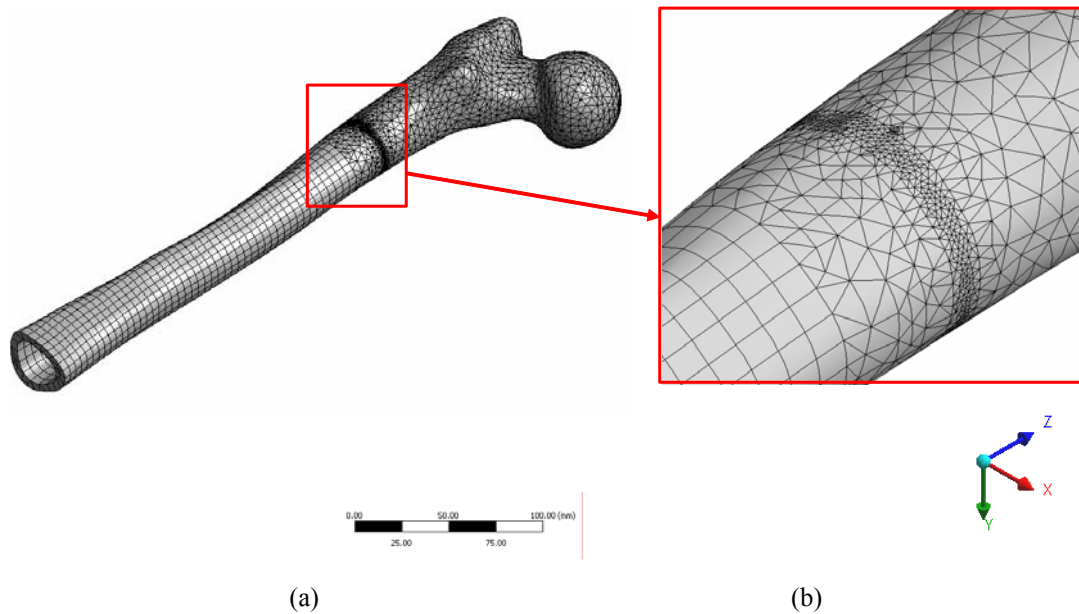


Figure 7. (a) Mesh of finite element model of a human femur and (b) mesh detail.

Note at cross section of interest, view fig. 7.b, the mesh is more refined to produce more reable results. Figure 8.a shows results of post-processing and shows a customary way of presentation of finite element results, in this case for maximum principal stress. Fig.8.b shows a alternative way of representing the same variable, but only accompanying a line of points positioned at exterior of chosen cross section.

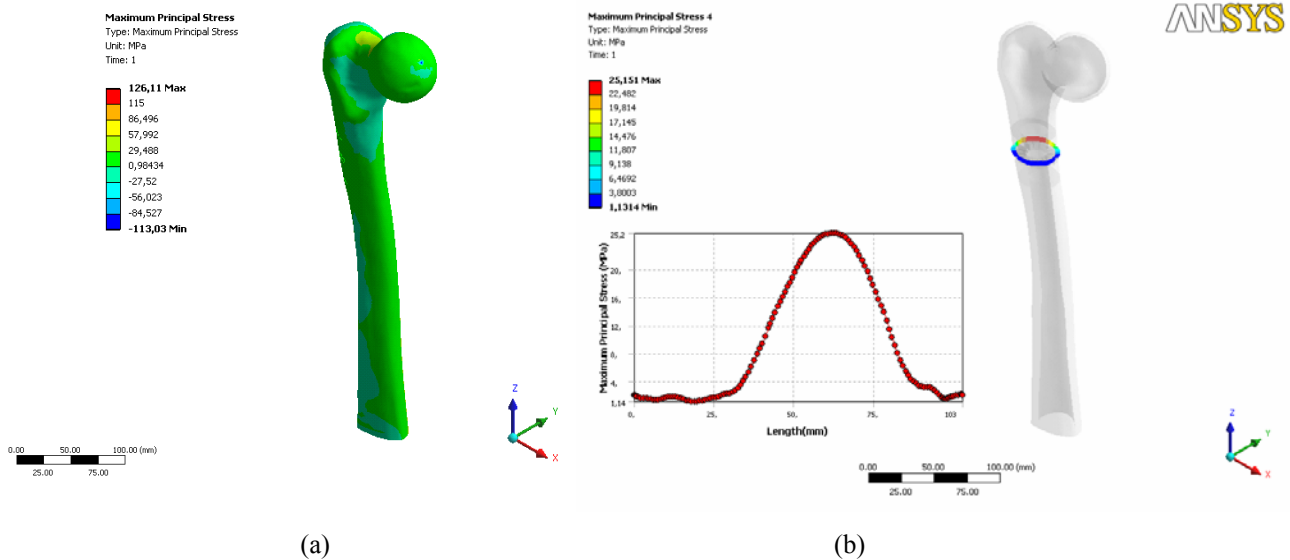


Figure 8. Example of numerical results: (a) standard postprocessing result and (b) path results.

Note that at fig.8.a the customary way of representing results leads only to a rough estimative of developed stresses of a determined region. At fig. 8.b the utilization of a predetermined path, the estimative of stresses are made in a more efficient way, allowing to describe stresses in function of angle γ (generating a graphical representation). Note that the finite element software increases the angle γ in clockwise pattern while the analytic models increase the same angle in an anticlockwise pattern.

4. COMPARATIVE STUDY

Figure 9.a shows the cross section of the hollow circle model, fig. 9.b shows the cross section of the hollow ellipse model and 9.c shows a cut at the chosen section of the human femur that was scanned from a real specimen. These three cross sections are approximately at same scale and the angle φ between coordinate systems is $8,98^\circ$. Note that at fig. 9.c the point of view is from the cross section to the femur's head.

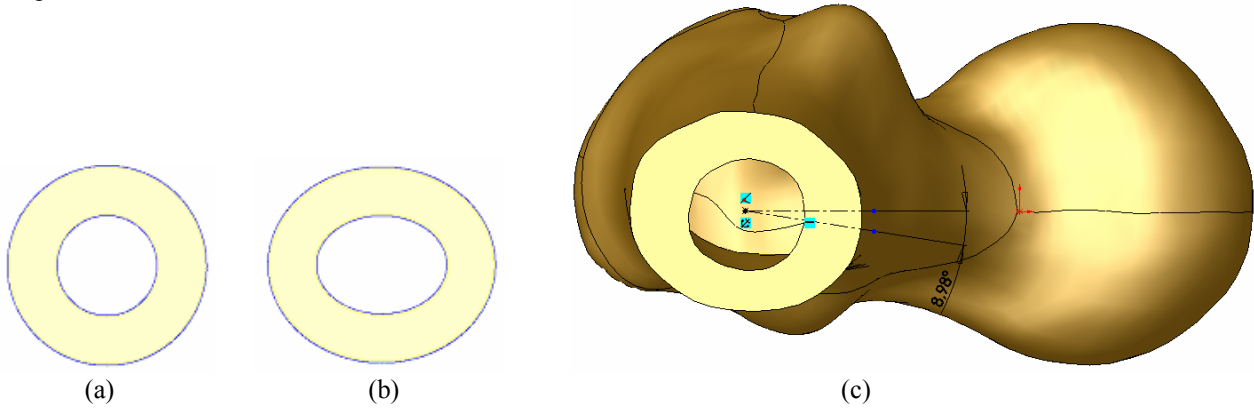


Figure 9. Cross sections: (a) hollow circle model, (b) hollow ellipse model and (c) real cross section of a human femur.

Note that although the external surface at fig. 9.c is similar to the hollow ellipse model, the internal surface is more similar to hollow circle model. To compare the performance of the two analytic models, using the F.E. model as reference, a real loading data provided by (Bergmann, 2001) was used. The loading and geometric variables are: $P_x^* = -420 N$, $P_y^* = -420 N$, $P_z^* = -1625 N$, $d_x = 0,069 m$, $d_y = -0,0014 m$, $d_z = 0,122 m$ and $\varphi = 8,98^\circ$. For the hollow circle model $r^c = 0,015 m$ and $t = 0,0075 m$; and for the hollow ellipse model $a = 0,0175 m$, $b = 0,015 m$ and $t = 0,0075 m$. Figure 10 shows a comparative diagram.

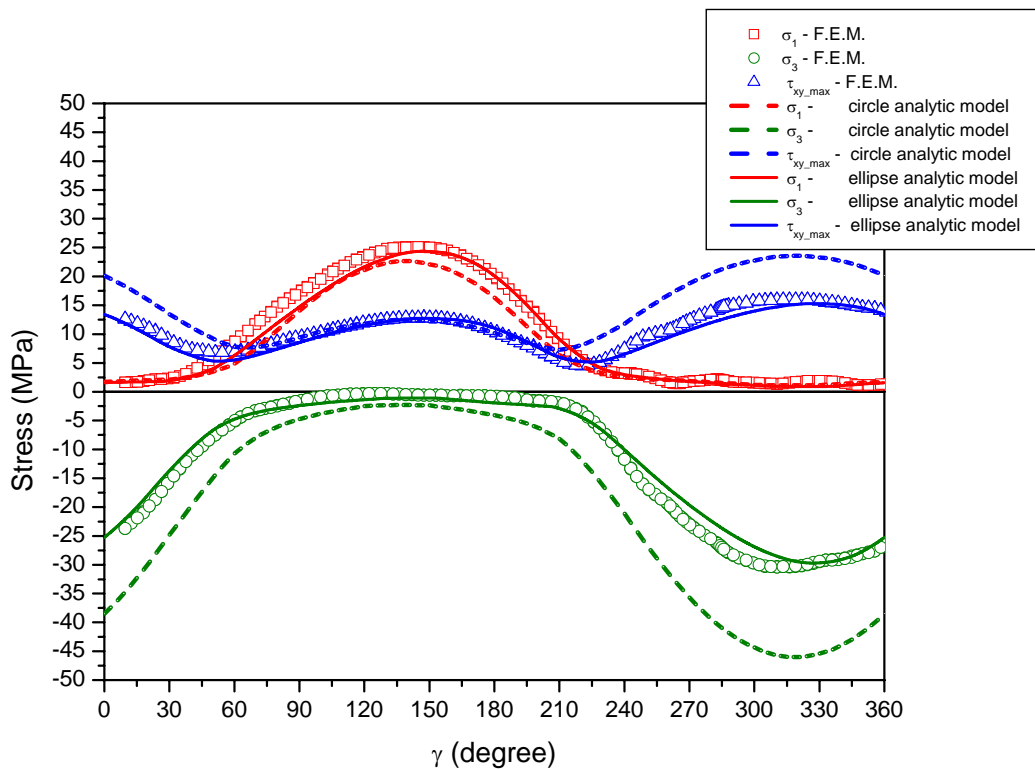


Figure 10. Comparative diagram of results of two analytic and a FE models.

Figure 10 shows the results of stresses (σ_1 , σ_3 and $\tau_{xy, \max}$) for points positioned at external surface of a determined cross section of a human femur for three models: one F.E. model, used as reference, and two analytic models, the hollow circle and the hollow ellipse models. It is apparent that the two analytic models generate results that are close to F.E. results. The hollow circle model has a simplest implementation but as shows fig. 9, only describes roughly the real cross of a long bone. This geometric ambiguity results in only a loose estimative of stresses. As the cross section of the hollow ellipse model approximates of real cross section geometry, as shown at fig.9, the estimation of stresses becomes more accurate, compensating the extra work required in its implementation.

5. CONCLUSIONS

Two simple analytic models were developed, with limiting hypothesis, to describe the distribution of principal and maximum shear stresses and its respective angles, at external surface of a human long bone, submitted to a static loading. The performance of analytic model was improved, with the utilization of an hollow elliptical shape to model a cross section of a medial long bone, in comparison with early analytic models with hollow circular shape. The results of application of hollow ellipse model showed good agreement with F.E. results, used as reference. The estimative of principal and maximum shear stresses at external surface of long bones, without the necessity of the utilization of a Finite Element software, is the major goal of this work.. This stresses results can be also used as input variables to a failure criterion for long bones.

6. REFERENCES

- Bayraktar, H.H., Morgan, E.F., Niebur, G. L., Morris, G. E., Wong, E.K, and Keaveny, T. M., (2004), "Comparison of the elastic and yield properties of human femoral trabecular and cortical bone tissue", *J. Biomech.*, Vol. 37, pp. 27-35.
- Bergmann, G., Deuretzbacher, G. Heller, M., Graichen, F., Rohlmann, A., Strauss, J. and Duda, G. N., (2001), "Hip contact forces and gait patterns from routine activities", *J. Biomech.*, Vol. 34, pp.859-871.
- Cilingir, A. C., Ucar, V. and Kazan, R., (2007), "Three-Dimensional Anatomic Finite Element Modeling of Hemi-Arthroplasty of Human Hip Joint", *Trends Biomater. Artif. Organs.*, Vol. 21, No. 1, pp. 63-72.
- Crandall, S.H., Dahl, N. C. and Lardner, T. J., (1978), "An Introduction to the Mechanics of Solids", Second Edition with SI units, Mc Graw Hill International Editions.
- Doblaré, M., García J. M. and Gómez, M. J., (2004), "Modeling bone tissue fracture and healing: a review", *Engineering Fracture Mechanics*, Vol. 71, pp. 1809-1840.
- Kenedi, P.P., Riagusoff, I.I.T., (2009), "Analytic and finite element models of a human long bone", In: *Anais do 2º Encontro Nacional de Engenharia Biomecânica, ENEBI 2009, Florianópolis, Santa Catarina, 6-8 Mai.*
- Kenedi, P.P., Riagusoff, I.I.T., (2008), "A Model of Stress Analysis of a Human Long Bone", In: *Anais do 21º Congresso Brasileiro de Engenharia Biomédica, CBEB 2008, Salvador, Bahia, 16-20 Nov.*
- Kenedi, P.P., Riagusoff, I.I.T., (2007b), "A Comparative Analysis of Failures Criteria Applied to Long Bones", In: *Proceedings of 19th COBEM, Brasilia, 5-9 Nov.*
- Kenedi, P.P., Riagusoff, I.I.T., (2007a), "Modeling initial fracture patterns in human long bones", In: *Anais do 1º Encontro Nacional de Engenharia Biomecânica, ENEBI 2007, Petrópolis, Rio de Janeiro, 23-25 Mai.*
- Keyak, J. H., Rosi, S.A., (2000), "Prediction of femoral fracture load using finite element models: an examination of stress – and strain-based failure theories", *J. Biomech.*, Vol. 33, pp. 209-214.
- Pettryl, M., Herf, J. and Fiala, P., (1996), "Spatial Organization of the Haversian Bone in Man", *J. Biomech.*, Vol. 29, No. 2, pp. 161-169.
- Rapoff, A.J., (2007), "engineering.union.edu/~rapoffa/MER440/Module%205/Representative%20Properties%20of%20Bone.pdf"
- Rudman, K.E., Aspden, R.M. and Meakin, J.R., (2006), "Compression or tension? The stress distribution in the proximal femur", *Biomedical Engineering Online*, vol.5, No.12.
- Spiegel, M.R., (1992), "Manual de Fórmulas, Métodos e Tabelas de Matemática", 2ªEdição, Makron Books.

7. RESPONSIBILITY NOTICE

The authors are the only responsible for the printed material included in this paper.